Theory of even-parity states and two-photon spectra of conjugated polymers

P. C. M. McWilliams, G. W. Hayden, and Z. G. Soos

Department of Chemistry, Princeton University, Princeton, New Jersey 08544

(Received 19 July 1990)

The two-photon absorption (TPA) spectrum of interacting π electrons in conjugated polymers is shown to be qualitatively different from any single-particle description, including the Hartree-Fock limit. Alternating transfer integrals $t(1\pm\delta)$ along the backbone lead to a weak TPA below the one-photon gap E_g for arbitrarily weak correlations at $\delta=0$, for intermediate correlations at $\delta=0.07$ in polyenes, and for strong correlations at any $\delta<1$. More intense TPA is derived from two-electron transfer across E_g; this even-parity state shifts from $2E_g$ in single-particle theory to E_g in the limit of strong correlations in Hubbard models and is around $1.5E_g$ for Pariser-Parr-Pople (PPP) parameters. The PPP model, which accounts for one- and two-photon excitations of finite polyenes, is extended to even-parity states in polydiacetylenes (PDA's), polyacetylene (PA), and polysilanes (PS's). Previous experimental data for PDA and PS support both the strong TPA above E_g and weak TPA slightly below E_g for $\delta=0.15$ in PDA and above E_g for $\delta\sim0.3$ in PS. The strong TPA expected around $1.5E_g$ in isolated PA strands shifts to $\sim E_g$ due to interchain π-electron dispersion forces. TPA intensities in correlated states are shown to reflect both ionicity and mean-square charge separation. The even-parity states of conjugated polymers, like those of polyenes, show qualitatively different features associated with electron-electron correlations.

I. INTRODUCTION

Conjugated polymers have recently been shown to have large, ultrafast nonlinear optical (NLO) responses associated with delocalized π electrons.[1] Both conjugated molecules and polymers have been intensively studied[2] in order to exploit this response, observed, for example, in third-harmonic generation (THG). Such molecular engineering presupposes an understanding of the virtual excited states that occur in NLO coefficients. We focus in this paper on the subset of virtual states corresponding to two-photon processes and demonstrate some qualitatively different features due to electron-electron (e-e) correlations.

Direct two-photon absorption (TPA) is well known[3] in finite polyenes, and the TPA spectrum has recently been obtained[4] for a spun, optical-quality polydiacetylene (PDA) film. Indirect assignments are based on techniques such as fluorescence, two-photon resonances in THG, three-wave mixing in solution, and electroabsorption or electroreflectance in solids. The position of an excited state with the same parity as the ground state is inferred in every case.

Conjugated polymers are complex systems whose electronic properties remain to be interrelated. Reports of two-photon processes differ sharply from polymer to polymer and even for different methods of detection in the same polymer. TPA in a PDA oligomer[5] and two-photon resonances in PDA crystals[6] or Langmuir-Blodgett films[7] are slightly but unequivocally below the optical gap E_g, while three-wave mixing[8] in solution and electroreflectance[9,10] in crystals place a two-photon PDA state well above E_g. The lowest TPA in polysilane (PS) films is almost 1 eV above E_g, as found both via fluores-

cence[11,12] and electroabsorption.[13] The PS spectrum[12,13] has another, more intense feature 1.2 eV higher. As discussed by Kohler,[14] the lowest TPA of finite polyenes is over 0.5 eV below the lowest one-photon absorption, and data up to 16-carbon polyenes extrapolate to around $E_g/2$ in polyacetylene (PA). The two-photon PA resonance[15] in THG, on the other hand, is at E_g.

Moreover, these diverse observations are completely unexpected in conventional band theories,[16] which predict a universal TPA spectrum as a function of $2\hbar\omega/E_g$. In Hückel or tight-binding theory, alternating transfer integrals $t(1+\delta)$ and $t(1-\delta)$ along the backbone lead to $E_g=4t\delta$ between a filled valence and an empty conduction band. In a long chain, states of both parity accumulate at E_g and the two-photon spectrum always peaks just above E_g, as shown in Fig. 1. There is no intensity at E_g since one- and two-photon selection rules are mutually exclusive.

The band-theoretical curve in Fig. 1 is a special case of the general problem solved by Agrawal, Cojan, and Flytzanis,[16] peaks at $(\frac{5}{4})^{1/2}E_g$, and is essentially independent of δ for $\delta<0.5$. The more idealized field-theoretical TPA spectrum of Wu and Kivelson[17] peaks at $(\frac{9}{8})^{1/2}E_g$ and is independent of δ. The points shown in Fig. 1 are the strongest TPA's of a 60-site Hückel chain with $\delta=0.33$. All three curves have been normalized to the same peak height. Absolute intensities are not typically obtained and even the one-photon gap is adjustable in solid-state models. Once chosen, E_g fixes the TPA spectrum in Fig. 1 for single-particle theory. These results also hold in mean-field theories, including the Hartree-Fock (HF) limit, and simply reflect the density of states at E_g.

We present here a unified approach[18] to TPA in conjugated polymers that accounts naturally for the differences
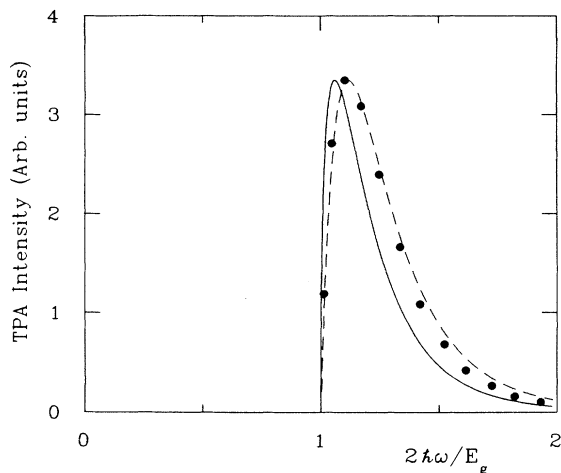
FIG. 1. TPA spectrum of conjugated polymers in the single-particle limit in units of the one-photon gap E_g. The solid points are for a 60-site chain with alternation $\delta=0.33$; the dashed line is from Ref. 16 with no lifetime broadening; the solid line is the field-theoretical result from Ref. 17. The same peak height was chosen for all three curves.

noted above for polyenes, PA, PDA's, and PS's and that differs qualitatively from the single-particle result in Fig. 1. We retain for simplicity the generic polymer with alternating transfer integrals and consider interacting π electrons[19] in Pariser-Parr-Pople (PPP) and Hubbard models. Exact solutions to finite segments are used throughout. Finite-size effects are minimized by relating TPA to the one-photon gap E_g that is independently known for conjugated polymers. The dipole transition moments of correlated states, in particular, provide crucial additional intensity information.

The theoretical understanding of TPA for interacting π electrons in linear chains is presented in Sec. II. Modest e-e interactions shift the lowest TPA below E_g for small δ and reduce its intensity. An alternation gap is quite general and remains even for the strong-correlation limit $U \gg t$ in the spin-wave spectrum. We also identify strong TPA to a particular A_g state derived from two-electron excitation across E_g. Such a state has previously been noted[20,21] to dominate the THG coefficient of finite polyenes and to have a large transition moment from the $|1\,^1B_u\rangle$ state at E_g. The two-electron state is around $1.5E_g$ for PPP parameters that fit the one- and two-photon spectra of finite polyenes and goes to $E_g \sim U$ in Hubbard models with $U \gg t$. The generality of these correlation effects is supported by an exact result for regular chains by projections onto single-particle states, by a sum rule for transition dipoles, and by the ionicity and mean-square charge separation of the ground and excited states.

We turn in Sec. III to the polymer data mentioned above. Now realistic parameters are essential, even for the rather qualitative comparisons that are presently possible. In practice, PDA's provide the greatest variety of two-photon processes, including TPA in films, THG in crystals and films, three-wave mixing in solution, and

electroabsorption and electroreflectance. The more limited PS data illustrate the shift of the lowest TPA above E_g with increasing alternation, again in contrast to the single-particle result in Fig. 1. The unshielded Coulomb interaction in PPP models leads to interchain dispersion forces among π electrons that are particularly important for PA, with its small interchain contacts.

As the simplest conjugated polymer, PA has been the focus of debate about the relative importance of e-e correlations,[1,22,19] just as polyenes were the testing ground for π-electron theories some 30 years ago. Negative spin densities and the different absorptions of charged and neutral solitons are correlation effects in PA. The one-photon absorption of[23] PDA's and[24] PS's is a singlet exciton, as demonstrated by the higher-energy threshold[25,26] for photoconduction in both cases, and correlations are essential for a bound electron-hole pair. As in polyenes, two-photon processes in conjugated polymers produce qualitatively different features associated with e-e correlations. The NLO responses discussed below involve virtual rather than real excitation, since all intense radiation is well below E_g. The formation of self-localized states[22] upon real excitations of conjugated polymers clearly requires electron-phonon (e-p) coupling, and vibronic effects are important for a detailed understanding of electronic structure in either conjugated molecules or polymers.

II. TWO-PHOTON ABSORPTION OF INTERACTING π ELECTRONS

A. One-dimensional Hückel, Hubbard, and PPP models

Microscopic expressions for NLO coefficients are obtained through perturbation theory, typically in the dipole approximation.[27,28] We consider here TPA in centrosymmetric polymers due to monochromatic radiation $\hbar\omega$ polarized along the chain. Similar expressions are readily found for other tensor components or for multicolor experiments. The ground state $|G\rangle$ and excited state $|Y\rangle$ both have even parity and the excitation energy $E(Y)$ is $2\hbar\omega_Y$. The TPA transition moment to $|Y\rangle$ is[28]

$$M(Y)=\sum_R \frac{\langle Y|\mu|R\rangle\langle R|\mu|G\rangle}{E(R)-\hbar\omega_Y}, \tag{1}$$

where μ is the component of the dipole operator along the backbone and the virtual states $|R\rangle$ with excitation energy $E(R)$ have odd parity. The TPA intensity is proportional to $|M(Y)|^2$. The sum over virtual states is difficult to evaluate for interacting many-electron systems.

As discussed elsewhere,[1,2] the NLO properties of conjugated molecules and polymers are associated with delocalized π electrons whose excitations[19] may be modeled separately from the σ framework. Each carbon has a Wannier orbital ψ_n based on a $2p_z$ orbital. Since the π electrons can be distributed among the ψ_n in only so many ways, the many-electron basis is large but finite. We may consequently rewrite (1) as[21]

$$M(Y)=\langle Y|\mu|\phi(-\omega_Y)\rangle \tag{2}$$

and treat the response function $\phi(-\omega_Y)$ directly in the

finite basis. It satisfies the linear inhomogeneous equation

$$(\mathcal{H} - E_G - \hbar\omega_Y)|\phi(-\omega_Y)\rangle = -\mu|G\rangle , \tag{3}$$

where $\mathcal{H}$ is the π electron Hamiltonian in the absence of radiation and E_G is its exact ground-state energy. The response function $\phi(\omega)$ has odd parity. In a finite basis, the direct solution of (3) is comparable to finding $|G\rangle$ exactly and is enormously simpler than obtaining the entire spectrum of virtual states in (1). Any NLO coefficient may be expressed in terms of response functions[29] of increasingly high order. Direct solutions[21] of inhomogeneous linear equations bypass entirely the sums over virtual states.

The π-electron Hamiltonian for a conjugated system contains one- and two-electron terms,

$$\mathcal{H} = \mathcal{H}_0 + \mathcal{H}_{ee} . \tag{4}$$

We begin with the Hückel or the tight-binding part $\mathcal{H}_0$ for a generic conjugated polymer with alternating transfer integrals $t(1+\delta)$ and $t(1-\delta)$ for partial double and single bonds, as sketched in Fig. 2. The second quantized expression for $\mathcal{H}_0$ is

$$\mathcal{H}_0 = \sum_{p,\sigma} -t[1-(-1)^p\delta]$$
$$\times (a_{p\sigma}^\dagger a_{p+1,\sigma} + a_{p+1,\sigma}^\dagger a_{p\sigma}) . \tag{5}$$

The fermion operator $a_{p\sigma}^\dagger$ $(a_{p\sigma})$ creates (annihilates) a π electron with spin σ at site p. We have taken equal site energies $\varepsilon_p = 0$ (Hückel α integrals) in (5) and restricted electron transfer as usual to adjacent sites. Both polyenes and polymers in Fig. 2 have a filled valence and an empty conduction band containing $N/2$ molecular orbitals (MO's) for N sites and $N_e = N$ π electrons. We label the conduction-band energies ε_r starting with $r = 1$ for the lowest unoccupied MO in Fig. 2 and the valence-band energies ε_{-r} starting with the highest occupied MO at $r = 1$. Since the parity alternates with increasing energy, the one-photon excitation from -1 to 1 defines the optical gap E_g for any length N.

The Hückel Hamiltonian (5) has alternancy symmetry[30] associated with a half-filled band with equal site energies and electron transfer between sites on two sublattices. This important symmetry is related to the electron-hole or charge-conjugation symmetry of interacting π-electron systems.[31] Quite generally, the valence and conduction orbitals of alternant systems are paired according to

$$\varepsilon_r = -\varepsilon_{-r} \quad \text{and} \quad c_{rn} = (-1)^n c_{-rn} , \tag{6}$$

where c_{rn} is the expansion coefficient of orbital r at site n. The alternancy relations (6) hold even when the coefficients are not known, for example, in an infinite chain with disordered t's. Moreover, the self-consistent treatment of $\mathcal{H}_{ee}$ in (4) for arbitrary PPP or Hubbard models also preserves the alternancy relations.[30] Thus $\langle \mathcal{H}_{ee} \rangle$ may be added to $\mathcal{H}_0$ in the following discussion of single-particle transition moments. The qualitatively different TPA of interacting π-electron systems will in fact be due to the fluctuation potential that is neglected in mean-field theory.

The important states in one-dimensional systems are close to E_g. The single particle states in Fig. 3 will serve to clarify one- and two-photon spectra of correlated states. The single-particle ground state $|G_0\rangle$ is a half-filled band for even N,

$$|G_0\rangle = \prod_{r=1}^{N/2} (a_{-r\alpha}^\dagger a_{-r\beta}^\dagger)|0\rangle , \tag{7}$$

where $|0\rangle$ is the vacuum state. The creation operators $a_{-r\sigma}^\dagger$ are the linear combinations of $a_{p\sigma}^\dagger$ that diagonalize (5) or, more generally, $\mathcal{H}_0 + \langle \mathcal{H}_{ee} \rangle$. As summarized in the Appendix, alternancy symmetry fixes many correlation functions of $|G_0\rangle$.

The lowest odd-parity state at $E_g = 2\varepsilon_1$ is

$$|1\,^1B_0\rangle = 2^{-1/2}(a_{1\alpha}^\dagger a_{-1\alpha} + a_{1\beta}^\dagger a_{-1\beta})|G_0\rangle , \tag{8}$$

where the subscript 0 designates single-particle states.
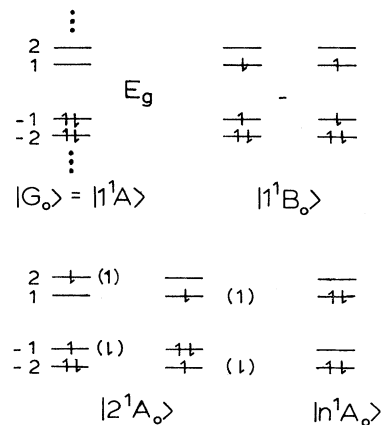
FIG. 3. Representative single-particle states of alternating chains. The one-photon excitation to $|1\,^1B_0\rangle$ has odd parity and e-h symmetry, while the other states have even parity and e-h symmetry. Two-electron excitation of $|n\,^1A_0\rangle$ at $2E_g$ involves high n in long chains, when there are many one-electron $g \rightarrow g$ or $u \rightarrow u$ excitations around E_g; e-e correlations in PPP chains mix $|2\,^1A_0\rangle$ and $|n\,^1A_0\rangle$.
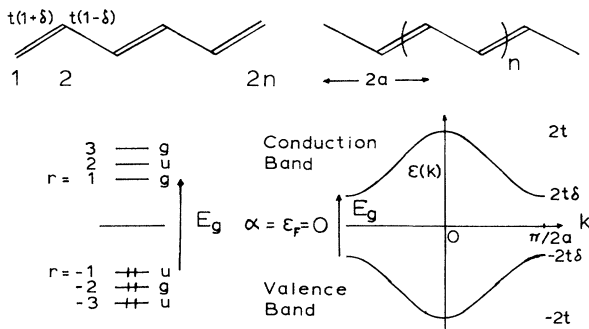

FIG. 2. Schematic representation of the valence and conduction MO's of finite and infinite polyenes with alternating transfer integrals $t(1\pm\delta)$ along the conjugated backbone. The optical gap E_g is the transition $r = -1$ to 1 for any length.

We have an odd linear combination of two Slater determinants. The even-parity states $|2\,^1A_0\rangle$ and $|n\,^1A_0\rangle$ in Fig. 3 contain four and one determinants, respectively, and have excitation energies of $\varepsilon_1+\varepsilon_2$ and $2E_g=4\varepsilon_1$. Since the $r=1$ and -1 orbitals are conjugate pairs, correlation functions and transition moments are again found analytically in the Appendix.

We consider next the $\mathcal{H}_{ee}$ term in (4). On-site interactions are kept in Hubbard models,[32]

$$\mathcal{H}_{\text{Hubbard}}=\sum_p Un_p(n_p-1)/2 \ , \tag{9}$$

where $n_p=a_{p\alpha}^{\dagger}a_{p\alpha}+a_{p\beta}^{\dagger}a_{p\beta}$ is the occupation number operator for site p and U is the same at every site. Increasing $U>0$ eventually localizes an electron on each site in half-filled Hubbard bands. The PPP model[33,19] has $V(0)=U$ and unshielded intersite Coulomb interactions at large separation,

$$\mathcal{H}_{ee}=\mathcal{H}_{\text{Hubbard}}+\tfrac{1}{2}\sum_{p,p'}{}' V_{pp'}q_pq_{p'} \ , \tag{10}$$

with $q_p=1-n_p$ and $p'=p$ excluded (as denoted by the prime on the summation). The coefficient $V_{pp'}$ depends on the distance $R_{pp'}$ between the sites in the Ohno interpolation,[34]

$$V(R)=U(1+R^2U^2/e^4)^{-1/2} \ . \tag{11}$$

Atomic data fix $V(0)=11.26$ eV for carbon. In contrast to extended Hubbard models, where intersite interactions are treated as adjustable parameters, the PPP choice (11) is supposed to hold for all hydrocarbons and illustrates a parameter-free phenomenological model.

Three- and four-center integrals in $\mathcal{H}_{ee}$ are neglected in the zero-differential-overlap (ZDO) approximation,[30,35] which is implicitly assumed in Hubbard, extended Hubbard, and PPP models. The dipole operator μ in (1) is site-diagonal in the ZDO approximation,

$$\mu=\sum_p ez_pq_p \ , \tag{12}$$

where z_p is relative to an arbitrary origin for a chain parallel to the z axis. The operator $q_p=(1-n_p)$ measures the π-electron charge at site p and is important for transition moments.

Once the π-electron Hamiltonian and the dipole operator are specified, we have explicit expressions for $M(Y)$ in (1) or for any NLO coefficient[21] in the dipole approximation. The direct solution of $\phi(-\omega)$ in (3) up to 12-site polyenes provides exact two-photon spectra for interacting π electrons in Hubbard or PPP models. The ground state $|G\rangle$ for centrosymmetric systems is an even-parity A_g singlet, while the one-photon excitation at E_g is an odd-parity singlet, $|1\,^1B_u\rangle$. Dipole selection rules imply TPA to $|m\,^1A_g\rangle$, with $m=2,3,\ldots$. We may specify the electron-hole (e-h) symmetry of $|G\rangle$ to be even, thereby fixing even and odd e-h symmetry for two- and one-photon excitations, respectively.

B. Characterization of correlated states

Although finite, the basis for half-filled Hubbard or PPP models increases almost as fast as 4^N with the poly-

mer length N. In the single-particle basis, correlations are treated via configuration interaction (CI) among Slater determinants such as those in Fig. 3. The CI expansion becomes exact when all configurations in a symmetry subspace have been included. The overlap $\langle Y|X_0\rangle$ is the CI coefficient of $|Y\rangle$ in the single-particle basis. The overlaps in Table I are for a PPP model of octatetrane, the eight-site polyene. Both the ground state $|G\rangle$ and the one-photon excitation to $|1\,^1B_u\rangle$ are semiquantitatively given by their single-particle counterparts in (7) and (8), respectively. The even-parity states $|2\,^1A_g\rangle$ and $|n\,^1A_g\rangle$ derived from the one- and two-electron states in Fig. 3, on the other hand, are strongly mixed and have opposite phases of the single-particle states. Such mixing indicates that TPA is more sensitive to correlations than the one-photon absorption at E_g.

Diagrammatic valence-bond (DVB) methods[36] provide an alternative, real-space basis of many-electron states. As suggested originally by Pauling, π-electronic states $|X\rangle$ are expressed as linear combinations of valence bond (VB) diagrams $|k\rangle$. Such diagrams contain a wealth of chemical insights. They also provide a simple method for automatically conserving the total spin S. All exact solutions for correlated states $|X\rangle$ or for response functions[21] $\phi(\omega)$ were obtained by DVB methods. The expansion coefficients c_{Xk} now correspond to the overlap $\langle X|k\rangle$. A great many diagrams are needed, however, and the physical content of such superpositions tends to be lost. We discuss several methods, in addition to the projections mentioned above, for characterizing correlated states involved in dipole transitions.

The representative VB diagrams in Fig. 4 are all six-electron singlets. A line between two sites indicates[37] a Heitler-London singlet between singly occupied sites, with vanishing charge operator $q_p=1-n_p$. Doubly occupied C^- sites are represented as crosses, while empty C^+ sites are dots. The Kekulé diagram $|1\rangle$ and diagrams $|2\rangle-|5\rangle$ are purely covalent, with $q_p=0$ at all p. As seen by inspection of the dipole operator in (12), purely covalent diagrams have vanishing transition moments and cannot contribute to either one- or two-photon spectra in the dipole approximation. The precise number of linearly independent covalent singlets for even N was found long ago by Rumer[38] and increases roughly as 2^N for large N. There are exactly five covalent singlets for $N=6$, shown in Fig. 4.

Purely covalent diagrams are consequently a small subset of the complete basis. Their importance lies in the fact that $|G\rangle$ and all 2^N spin states become purely co-

TABLE I. Overlap $\langle X_0|Y\rangle$ of Hückel and PPP eigenfunctions for an eight-site polyene. The Hückel states $|X_0\rangle$ are indicated in Fig. 3; the two-electron PPP excitation is $n=5$ for $N=8$.

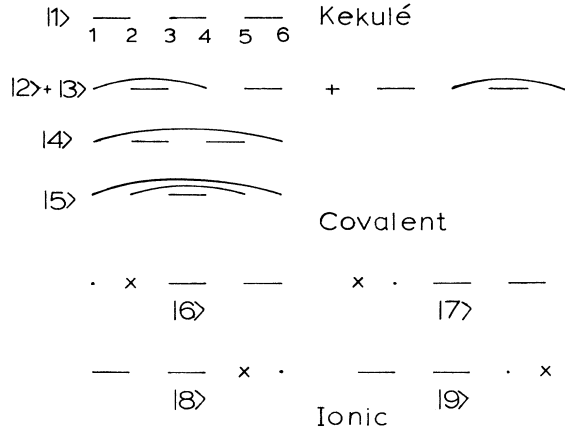|	$|G\rangle$	$|1\,^1B_u\rangle$	$|2\,^1A_g\rangle$	$|n\,^1A_g\rangle$
$\langle G_0|$	0.917	0.0	0.010	0.308
$\langle 1\,^1B_0|$	0.0	0.910	0.0	0.0
$\langle 2\,^1A_0|$	-0.155	0.0	0.612	-0.561
$\langle n\,^1A_0|$	-0.157	0.0	0.594	0.510

FIG. 4. Representative VB diagrams for a six-site chain. The Kekulé diagram $|1\rangle$ and diagrams $|2\rangle-|5\rangle$ give the complete set of purely covalent diagrams and form four A_g^+ states. The ionic diagrams $|6\rangle-|9\rangle$ have equal amplitudes and form linear combinations with A^+, A^-, B^+, and B^- symmetry.

valent in the atomic limit $U \gg t$ of Hubbard models, when all doubly occupied sites are excluded. Virtual contributions lead to antiferromagnetic exchange $J \sim t^2/U$ between adjacent $s = \frac{1}{2}$ sites. DVB solutions in the smaller subspaces with $S = 0, 1, 2, \ldots, N/2$ can be extended to longer spin chains.[39] In the present context, we note that charge fluctuations are completely suppressed in purely covalent diagrams, where q_p vanishes at all sites, and that all purely covalent singlets have the same e-h symmetry as $|G\rangle$.

Most VB diagrams are ionic, in the sense that they contain at least one doubly occupied or empty site. Diagrams $|6\rangle-|9\rangle$ in Fig. 4 are representative ionic diagrams with one ion pair. Each diagram is an eigenvector of (12), with eigenvalue μ_k given by assigning the indicated C^- and C^+ charges. Inversion and e-h symmetry fix the phases of $|6\rangle-|9\rangle$ and lead to an A^+, A^-, B^+, and B^- linear combination. Dipole selection rules connect A^+ with B^- or A^- with B^+. Since VB diagrams are automatically orthogonal unless their charge distributions coincide exactly, it follows that transition moments $\langle A^+|\mu|B^-\rangle$ depend only on the admixture of diagrams with identical charge distributions.[40] Furthermore, covalent singlets are rigorously excluded by e-h symmetry from any state in the B_u^- manifold.

The ionicity per site $Q(X)$ provides a quantitative measure of covalent and ionic contributions in state $|X\rangle$,

$$Q(X) = \sum_p \langle X|q_p^2|X\rangle/N . \tag{13}$$

Alternancy symmetry is shown in the Appendix to be sufficient for fixing $Q(X_0) = \frac{1}{2}$ in the single-particle states $|G_0\rangle$, $|2\,^1A_0\rangle$, and $|n\,^1A_0\rangle$ for any N. The ionicity of $|1\,^1B_0\rangle$ is greater than $\frac{1}{2}$ in finite systems. The ionicity of purely covalent diagrams, on the other hand, vanishes. The ionicities for PPP models of polyenes are seen in Table II to be intermediate, as expected, and closer to the single-particle limit. The conventional representation of

TABLE II. Ionicity per site, $Q(X)$ in Eq. (13), of exact polyene states of N-site PPP models with $\delta = 0.07$.

$|X\rangle$	$N=6$	8	10	12
$|G\rangle$	0.3524	0.3554	0.3574	0.3588
$|1\,^1B_u\rangle$	0.5267	0.4852	0.4623	0.4476
$|2\,^1A_g\rangle$	0.2769	0.3082	0.3243	0.3339
$|n\,^1A_g\rangle$	0.4412	0.4293	0.4176	0.3966

conjugated systems in Fig. 2 by their Kekulé structure is oversimplified. The q_p^2 operator in (13) is closely related to the Hubbard interaction in (9), since

$$q_p^2 = q_p + 2a_{p\alpha}^\dagger a_{p\beta}^\dagger a_{p\beta} a_{p\alpha} \tag{14}$$

and $\langle q_p \rangle = 0$ due to e-h symmetry. The second term in (14) is twice the on-site interaction in (9).

We consider next the mean-square charge fluctuations[18] in state $|X\rangle$,

$$W(X) = -\frac{1}{2} \sum_{p,p'} (z_p - z_{p'})^2 \langle X|q_p q_{p'}|X\rangle/N . \tag{15}$$

The sign reflects the attractive nature of Coulomb interactions. In a neutral system, $\sum_p q_p$ vanishes identically and so do the square contributions in (15). The cross terms are related to (12),

$$Ne^2 W(X) = \sum_{p,p'} e^2 z_p z_{p'} \langle X|q_p q_{p'}|X\rangle$$
$$= \sum_P |\langle P|\mu|X\rangle|^2 , \tag{16}$$

where the second equality follows from completeness. The mean-square charge separation $W(X)$ provides a sum rule[18] for the squares of all dipole transition moments from $|X\rangle$. We may consequently ascertain how completely a given set of correlated states exhausts the bound in (16).

We again illustrate with PPP models for polyenes. As shown in Table III, ground-state charge fluctuations are small, ~ 0.3 in units of the mean bond length $a = 1.21$ Å along the polymer backbone in Fig. 2. $W(1\,^1B_u)$ values are distinctly larger, as expected on producing an ion pair. $W(n\,^1A_g)$ is larger still for the state derived from two-electron excitation at E_g, whose index n depends on N. This clearly reflects increased charge separation, since Table II shows $Q(n\,^1A_g)$ to be less than $Q(1\,^1B_u)$.

The transition moments in Table III show that over 80% of the dipole intensity from $|G\rangle$ is to $|1\,^1B_u\rangle$. The one-dimensional nature of the chain, especially for small alternation, leads to a sharp peaking of the one-photon spectrum at E_g. This feature is retained by correlated states for transitions polarized along the chain.

The TPA transition moment $M(Y)$ in (1) will be restricted to low-lying ^1A_g states that are primarily connected to $|1\,^1B_u\rangle$, at least for the most important case of radiation polarized along the chain. The large transition moment from $|1\,^1B_u\rangle$ to the two-electron state $|n\,^1A_g\rangle$ in Table III is remarkable. As shown in the Appendix, single-particle states have equal transition moments from $|1\,^1B_0\rangle$ to either $|G_0\rangle$ or $|n\,^1A_0\rangle$, since the same MO's

TABLE III. Mean-square charge separation, $W(X)$ in Eq. (15), and dipole transition moments to $|1\,^1B_u\rangle$ in N-site PPP models for polyenes; a is the mean bond length along the polymer.

	$N=6$	8	10	12
$W(G)/a^2$	0.2660	0.2822	0.3167	0.3341
$|\langle 1\,^1B_u|\mu|G\rangle|^2/Ne^2a^2$	0.2420	0.2636	0.2802	0.2921
$W(1\,^1B_u)/a^2$	1.010	1.143	1.247	1.322
$|\langle 1\,^1B_u|\mu|n\,^1A_g\rangle|^2/Ne^2a^2$	0.6739	0.7718	0.8142	$0.7229+0.1722^a$
$W(n\,^1A_g)/a^2$	1.621	1.949	2.153	$2.066+0.677^a$
$W(2\,^1A_g)/a^2$	0.2344	0.2929	0.3354	0.3682

[a]Contribution from $|7\,^1A_g\rangle$, which is 0.1397 eV below $E(8\,^1A_g)$.

are involved. The phase relations between the exact and single-particle states in Table I are responsible for the large transition moment, and the opposite phases in $|2\,^1A_g\rangle$ lead to reduced TPA intensity and to reduced ionicity in Table II. Some 80% of the dipole intensity from $|1\,^1B_u\rangle$ is exhausted by the two transitions in Table III. The remaining 5×10^3 singlet A_g^+ states for $N=10$ or 5×10^4 states for $N=12$ are consequently known in advance to produce weak TPA's. A few exact states suffice for TPA in interacting systems for light polarized along the chain.

C. TPA and correlations in Hubbard chains

Variable e-e correlations in solid-state systems are understood in terms of Hubbard models, which capture the essential features through the ratio U/t of on-site interactions in (9) to the bandwidth $4t$. We begin with an exact result for the infinite regular ($\delta=0$) chain. Now the $U=0$, or Hückel, limit corresponds to a one-dimensional metal rather than a conjugated polymer. The optical gap $E_g=4t\delta$ and the two-photon gap both vanish. The TPA gap also vanishes for $U>0$ and involves $k=0$ excitations of homopolar singlets[41] whose spectrum was found exactly by Ovchinnikov. The gapless nature of covalent states in regular Hubbard chains is also shown by their finite magnetic susceptibility[42] at 0 K. The one-photon gap $E_g(t,U)$ to ionic singlets with the opposite e-h symmetry, on the other hand, is explicitly known[43] to be finite for any $U>0$. Even in the absence of information about intensities, TPA in regular Hubbard chains is qualitatively different from the single-particle spectrum in Fig. 1.

The inversion and e-h symmetries of half-filled quantum-cell models are retained[19] in alternating Hubbard, PPP, or other chains with spin-independent e-e interactions $V(R)$. Finite alternation ($\delta>0$) produces a gap in the $^1A_g^+$ manifold as discussed[44,39] in the large-U limit of alternating Heisenberg spin chains and of triplet spin excitons.[45] The alternation or covalent gap between $|G\rangle$ and $|2\,^1A_g\rangle$ thus reflects $\delta>0$. The one-photon gap to $|1\,^1B_u\rangle$ involves a subspace with different e-h symmetry, contains both correlation and alternation contributions, and does not vanish as $\delta\to0$. Symmetry considerations thus establish different one- and two-photon gaps, neither of which is known exactly in alternating Hubbard or PPP chains.

To follow the evolution of the TPA spectrum with increasing U, we chose a six-site Hubbard chain with large

alternation $\delta=0.50$ and obtained the transition moments $M(Y)$ in (1). The $U=0$ panel in Fig. 5(a) shows the two even-parity excitations to $2\,^1A_0$ and $3\,^1A_0$ to occur at $2\hbar\omega<2E_g$ for large δ. The next-higher even-parity singlet, with $n=4$, is the two-electron transfer $|n\,^1A_0\rangle$ in Fig. 3. At intermediate correlations $U=2t$, in Fig. 5(b), the $4\,^1A_g$ state drops below $2E_g$. The $2\,^1A_g$ and $3\,^1A_g$ features shift to lower energy relative to E_g and lose intensity. These trends are even more marked in the $U=4t$ panel, where $2\,^1A_g$ is now below E_g. Since there are 56 states in the singlet $^1A_g^+$ manifold for $N=6$, and thus 55 TPA's, we expect a large number of less intense transitions.

The situation is simpler at $U=8t$, in Fig. 5(d), where weak spin waves at energies of the order of t^2/U are clearly seen. As previously mentioned, there are five purely covalent singlets for $N=6$ that lead to four ^1A_g combinations in Fig. 4 and thus to three TPA's. The
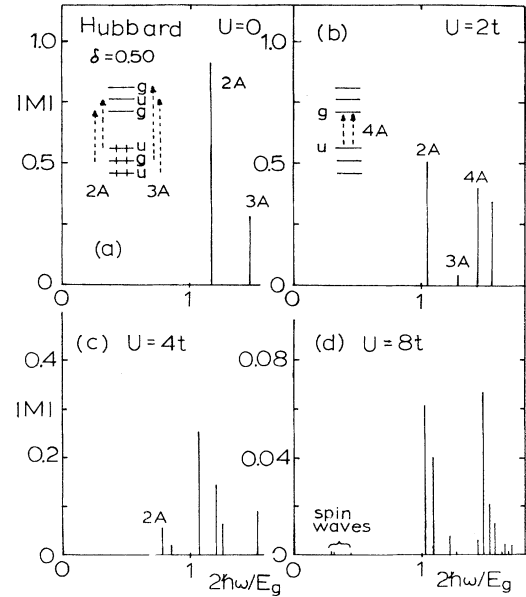

FIG. 5. Exact two-photon transition moments $M(Y)$ in Eq. (1) for $n\,^1A_g$ states below $1.8E_g$ in a six-site Hubbard chain, with alternation $\delta=0.50$ and $U=0$, $2t$, $4t$, and $8t$, respectively. (a) Single-electron transitions are identified; (b) double excitation at the one-photon gap E_g; (d) three spin-wave excitations. Note the scale changes in (c) and (d).

number of spin-wave excitations at $U \gg t$ is easily predicted for any N. Their greatly reduced intensity follows naturally from their predominantly covalent character, which requires that all dipole moments in (1) be due to small ($\sim t/U$) admixtures of ionic diagrams. The more intense transitions above E_g at $U = 8t$ are to more ionic $^1A_g^+$ states, which contain significant contributions from diagrams $|6\rangle - |9\rangle$ in Fig. 4. In the large-U limit, $E_g \sim U$ and states with a single ion pair give a TPA spectrum at $2\hbar\omega = E_g$ whose fractional width is $\sim 4t/U$. We then have a filled band of spinless fermions whose TPA resembles the Fig. 1 spectrum for a half-filled band of noninteracting $s = \frac{1}{2}$ fermions.

The Hubbard dimer has only one TPA, the two-electron excitation at $2E_g = 4t$ in the $U = 0$ limit. Now $|2\,^1A_g\rangle$ is always derived from the two-electron excitation and analytical results are available for both the energies and intensities. The dimer TPA at $2\hbar\omega_Y$ satisfies

$$E_g/\hbar\omega_Y = 1 + [1 + (4t/U)^2]^{-1/2} . \qquad (17)$$

As expected, $2\hbar\omega_Y = E(2\,^1A_g)$ goes from $2E_g$ at $U = 0$ to E_g at $U \gg t$. There are only two dipole transition moments in (1) for the dimer, from $|G\rangle$ to $|1\,^1B_u\rangle$ and from $|1\,^1B_u\rangle$ to $|2\,^1A_g\rangle$. Their ratio goes as $\tan\theta$, with $2\theta = \arctan(4t/U)$. The second transition moment is larger for $U > 0$.

The ionicity Q and mean-square charge separation W of Hubbard chains with alternation $\delta = 0.07$ are compared in Table IV for $U = 2t$ and $4t$ with the Hückel ($U = 0$) results. Hubbard models proposed[46] for PA typically have U around $2t$ and $\delta \sim 0.10$. Even modest correlations reduce the ground-state ionicity in Table IV, as expected from a larger admixture of purely covalent diagrams. No such diagrams occur in $|1\,^1B_u\rangle$ due to e-h symmetry and its ionicity is indeed less sensitive to U. The $W(G)$ results in Table IV at $U = 2t$ are nearly equal to the PPP values in Table III, consistent with their similar ionicities. On the other hand, $W(1\,^1B_u)$ for $U = 2t$ Hubbard models is almost twice the PPP result. Coulomb attraction between the ion pair reduces charge separation in the PPP model.

We summarize briefly the principal features of TPA in Hubbard models. There is no gap in the two-photon spectrum of $\delta = 0$ chains for any U, while E_g is finite for

$U > 0$. In the dimer limit ($\delta = 1$), on the other hand, TPA is always above E_g and approaches E_g at $U \gg t$. For $0 < \delta < 1$, weak TPA to spin waves occurs below E_g for sufficiently large U, but the one- and two-photon gaps are comparable at small U. The universal nature of the single-particle spectrum in Fig. 1 disappears completely in Hubbard models and hence in PPP models. Either model suffices for understanding e-e effects on TPA. The PPP model has the additional merit of accounting for the one- and two-photon excitations of finite polyenes and is consequently the model of choice for polymers.

D. Alternation and size dependence in PPP chains

We adopt standard microscopic parameters for PPP models of hydrocarbons:[19] $t = -2.40$ eV and $\delta = 0.07$ in (5), $U = V(0) = 11.26$ eV in (9), partial single and double bonds of 1.45 and 1.35 Å in Fig. 2, and intersite interactions in (11). Although approximate, the consistent use of a single-parameter set facilitates theoretical comparisons. Since the crossover to e^2/R in (11) depends on the size of U, we examined correlation dependence in PPP models by varying t at fixed U. The qualitative features of the TPA spectra of Hubbard models are found, as expected. In particular, the two-electron excitation $|n\,^1A_g\rangle$ shifts from $\sim 2E_g$ at large t, in the less correlated system, to E_g at small t, when correlations are strong. We consider here the alternation and size dependences of the TPA spectrum.

The transition moments $M(Y)$ in (1) are plotted against $2\hbar\omega/E_g$ in Fig. 6 for polyenes of length $N = 6$, 8, 10, and 12, using the above parameters. The logarithmic scale brings out the weak transitions. Since the TPA intensity goes as $|M(Y)|^2$, the spectra in Fig. 6 are clearly dominated by the $|n\,^1A_g\rangle$ states with $n = 4$, 5, 6, and 8 with increasing N. The $4\,^1A_g$ state for $N = 6$ is derived from the two-electron excitation in Fig. 3, as discussed for Hubbard chains in Fig. 5(b). For other N, the strongest TPA is also derived from the two-electron excitation. The similar character of these two-electron states is confirmed by the systematic variation of ionicities in Table II and mean-square charge separations in Table III, as well as projections onto single-particle states shown in Table I.

The strong TPA may be simply understood by noting that the single-particle spectrum has strong divergences for $2\hbar\omega \geq 2E_g$, but the coincidence of one- and two-photon processes precludes experimental study. The single-particle state $|n\,^1A_0\rangle$ in Fig. 3 has a large transition moment in (1) and a divergent denominator at $\hbar\omega = E_g$. Correlations shift the two-electron state to lower energy into the experimentally accessible range. As indicated in (17) for Hubbard dimers, the red shift of $|n\,^1A_g\rangle$ increases with increasing correlations and saturates at E_g for $U \gg t$. The PPP correlations are seen to be intermediate.

The $7\,^1A_g$ and $8\,^1A_g$ excitations in the $N = 12$ panel in Fig. 6 are particularly striking. Exact solution of the PPP model gives a 0.140 eV splitting, which is just a few percent of $E_g = 4.009$ eV. There are almost 57 000 symmetry-adapted $^1A_g^+$ linear combinations of VB dia-
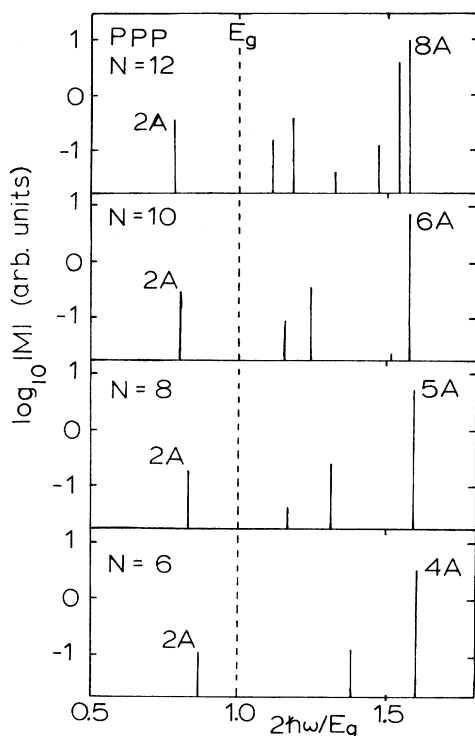
TABLE IV. Ionicity per site Q in Eq. (13) and mean-square charge separation W in Eq. (15) for N-site Hubbard models with $U = 2t$ (upper entry) and $U = 4t$ (lower entry), relative to the $U = 0$ Hückel value.

	$N = 6$	8	10
$Q(G)/Q(G_0)$	0.6430	0.6542	0.6614
	0.3716	0.3798	0.3848
$Q(1\,^1B_u)/Q(1\,^1B_0)$	0.8172	0.7855	0.7664
	0.7179	0.6529	0.6104
$W(G)/W(G_0)$	0.5362	0.5200	0.5057
	0.2414	0.2167	0.1981
$W(1\,^1B_u)/W(1\,^1B_0)$	0.9537	0.9522	0.9530
	0.9160	0.9075	0.9033

FIG. 6. Exact two-photon transition moments, $\log_{10}|M(Y)|$ in Eq. (1), for $n\,{}^1A_g$ states below $1.8E_g$ in N-site PPP models with alternation $\delta=0.07$ and polyene parameters; E_g is the one-photon gap.
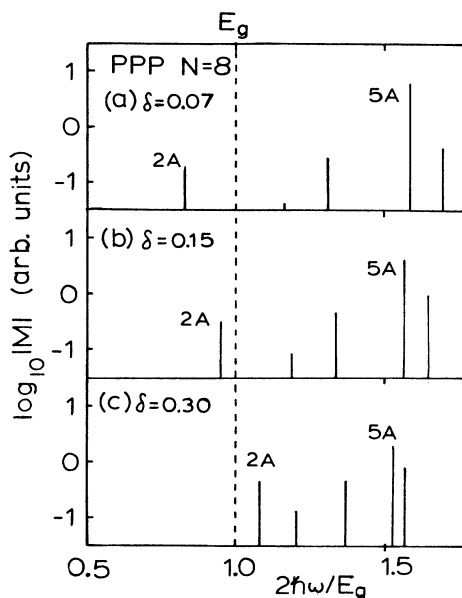
FIG. 7. Exact two-photon transition moments, $\log_{10}|M(Y)|$ in Eq. (1), for $n\,{}^1A_g$ states below $1.8E_g$ in an eight-site PPP model with $\delta=0.07$, 0.15, and 0.30 and otherwise unchanged polyene parameters and geometry.

grams corresponding to over 2.7×10^6 Slater determinants with $S_z=0$. The $7\,{}^1A_g$ and $8\,{}^1A_g$ ionicities are similar, 0.318 and 0.397. Yet their mean-square charge separations are quite different, with $W(7\,{}^1A_g)=0.991$ Å^2 and $W(8\,{}^1A_g)=3.025$ Å^2, and their relative TPA intensities are $(4.089/9.081)^2=0.203$. Such intensity variation between nearby levels in small systems suggests that resolved TPA bands may occur in polymers.

Small $M(2\,{}^1A_g)$ values relative to $M(n\,{}^1A_g)$ are directly linked to the admixture of single-particle states shown in Table I for $N=8$. Some 60% of either $|2\,{}^1A_g\rangle$ or $|n\,{}^1A_g\rangle$ comes from the corresponding single-particle states, with opposite phases. These phase relations for single-particle states are shown in the Appendix to result in smaller ionicity, smaller charge separation, and smaller transition moments for $2\,{}^1A_g$. The less ionic nature of $|2\,{}^1A_g\rangle$ than $|G\rangle$ in Table II is by no means obvious without such phase information.

The triple bonds in the PDA backbone lead to greater alternation, which is represented[16] by an effective $\delta\sim0.13$. We took $\delta=0.15$ and retained the polyene geometry in Fig. 6. We likewise retain the same geometry and polyene parameters in $\delta=0.30$ chains to illustrate the larger alternation of σ-conjugated PS chains. PPP results[47] to $N=12$ for the actual geometry and Si parameters are similar. The alternation dependence of the TPA spectrum of $N=8$ chains is shown in Fig. 7. The $2\,{}^1A_g$ feature shifts to higher energy and becomes more intense with increasing δ. The $|2\,{}^1A_g\rangle$ state

remains above $|1\,{}^1B_u\rangle$ at these intermediate correlations,[47] even on extrapolating against N^{-1} using data to $N=12$. A two-photon gap below E_g at large δ requires stronger e-e correlations.

The strongest TPA, $5\,{}^1A_g$ in Fig. 7, become less intense with increasing δ. It remains the strongest feature even at $\delta=0.30$ and is still above $1.5E_g$. The N dependence is rather weak, in the range from 1.60 to $1.55E_g$ in Fig. 6 on going from $N=6$ to 12. We expect the two-electron feature to remain above E_g in the infinite chain, around 1.4–$1.5E_g$ for polyenes. The dimer TPA in (17) is at $1.382E_g$ for $U=2t$ and is consistent with the strength of e-e correlations fixing, to a first approximation, the position of the two-electron TPA.

III. EVEN-PARITY STATES IN CONJUGATED POLYMERS

Several comments are in order before turning to the PA, PDA, and PS experiments mentioned in the Introduction. These polymers approximate best the generic model in Fig. 2, contain neither heteroatoms nor rings in their conjugated backbones, and have been the most extensively characterized both experimentally and theoretically. The analysis[1] of polymers with rings or heteroatoms usually involves modifications of the generic polymer and presupposes the same qualitative picture. We consider the simplest cases to demonstrate a consistent picture for two-photon processes that have previously been treated separately and phenomenologically.

Our goal is to identify common features among different polymers. The internal reference provided by the one-photon gap E_g greatly facilitates the assignment of two-photon features. Fully quantitative analyses of

two-photon spectra will require additional information about vibronic effects, backbone conformations, side-group coupling, and interchain or solvent interactions.

As noted in the Introduction, there are several approaches to the identification of even-parity states in conjugated polymers. Polyene parameters for PPP segments lead to qualitatively different TPA spectra, as shown in Figs. 6 and 7, from the single-particle result in Fig. 1. We reexamine NLO data for evidence of an intense TPA around $1.5E_g$ and weak TPA, at the alternation gap, below E_g for small δ and above E_g for large δ. The greatest variety of experiments involving even-parity states in conjugated polymers have been carried out on PDA's.

A. Polydiacetylenes

The availability of many PDA's as single crystals[48] is a major advantage for detailed experimental characterization. Their nondegenerate $\mathrel{\mathop{\rule{0pt}{0pt}}\limits^{}} CR\!-\!C\!\equiv\!C\!-\!CR\mathrel{\mathop{\rule{0pt}{0pt}}\limits^{}}_n$ backbones, where R represents nonconjugated side groups, are more difficult to model than the generic polymer in Fig. 2. Correlations have long been recognized[23] to be essential in PDA's; the excitonic absorption at $E_g \sim 2$ eV is some 0.4 eV below the threshold for photoconduction.[25] The larger alternation due to the triple bond leads to an effective $\delta \sim 0.15$, the value used below. The large R groups chemically isolate the conjugated backbones, typically to interchain separations of 7–10 Å.

The conjugation length is nominally infinite in crystals and sharp spectra are found, especially at low temperature. The PDA-PTS absorption at 2.0 eV at 300 K has a width of 100 meV and fixes E_g accurately. Below the structural transition at 190 K, two crystallographically inequivalent strands[49] are split by 40 meV and each line is ~ 15 meV wide at 15 K. Electronic one dimensionality is confirmed through pump-probe experiments[49] that show the exciton to be confined to one strand during its < 2-ps lifetime.[50]

The sharp (~ 100 meV) resonance[6] at 1.80 eV in the THG spectrum of PDA-PTS crystals thus unequivocally demonstrates even-parity states below E_g. This band corresponds to the alternation gap in the present model. In a static electric field, even- and odd-parity states are mixed and a one-photon transition to $|2\,^1A_g\rangle$ become allowed. Sebastian and Wieser[51] found a sharp (~ 50 meV) feature at 1.75 eV in the electroabsorption spectrum of a thick (0.35 mm) PDA-PTS crystal, about 0.2 eV below the intense absorption at E_g. Rather than a defect state, as originally suggested,[51] we assign the 1.75-eV absorption to $|2\,^1A_g\rangle$.

THG and electric-field-induced second-harmonic (EFISH) generation on Langmuir-Blodgett films[7] of several other PDA's indicate even-parity states some 0.1 to 0.3 eV below E_g. The $|2\,^1A_g\rangle$ state is[5] 1700 cm^{-1} (0.21 eV) below the one-photon 0-0 line at 3.26 eV in an $N = 14$ PDA oligomer, whose larger E_g reflects a shorter conjugation length. Both the fluorescence and absorption show rich vibronic structure at 77 K in an alkane matrix.[15] The unambiguous molecular assignment thus parallels the polymer spectra and shows the alternation

gap in PDA's to be slightly smaller than E_g. More quantitative treatments must include vibronic coupling, the specific role of the side groups R, and interactions with the solvent or the solid-state environment. Variations of ~ 0.2 eV in the $E(2\,^1A_g)$-E_g splitting for PDA's are quite acceptable for the present model.

We turn next to previous evidence for strong TPA around $1.5E_g$, as shown in the $\delta = 0.15$ panel of Fig. 7. Chance et al.[8] reported three-wave mixing (3WM) for 3- and 4-butoxycarbonylmethyl urethane (BCMU) solutions in several solvents. The backbone conformation and conjugation lengths must now be modeled, but interchain interactions are clearly minimal. Their red, yellow, and blue solutions are striking evidence for variations in E_g. To fit the 3WM data, they chose a three-state model: a ground state $|G\rangle$, an odd-parity state at E_g that corresponds to $|1\,^1B_u\rangle$, and another even-parity state that we assign as $|n\,^1A_g\rangle$. Its position, in units of E_g, is 1.43 in the yellow solution, 1.49 in the red solution, and 1.3 or 1.46 for two fits to the blue solution.

The oscillator strength f from $|1\,^1B_u\rangle$ to $|n\,^1A_g\rangle$ was found[8] to be about twice as large as to $|G\rangle$. The corresponding ratio of transition moments squared in Table III is around 3 and leads to an f ratio of 1.5 when the upper state is at $1.5E_g$. The intensity information is particularly compelling evidence for correlations in view of the equal transition moments from $|1\,^1B_0\rangle$ to $|G_0\rangle$ and $|n\,^1A_0\rangle$ for the single-particle states in Fig. 3. Interacting π electrons in PPP strands provide a microscopic picture for the 3WM and for previous[52] PTS and poly[5,7-decadiyne-1,12 diol-bis-phenylurethane] (TCDU) data that Chance et al.[8] reinterpreted in terms of a single A_g state above E_g.

The fit for the half-width Γ of the upper A_g state was[8] about 0.5 eV, or $\sim 20\%$ of E_g. Even qualitative analysis of polymer spectra requires broadening parameters associated with excited-state lifetimes, with conformational disorder leading to a distribution of conjugation lengths, or with an inhomogeneous environment. While disorder leads to Gaussian broadening, we approximate all broadening by the Lorentzian widths that describe excited-state lifetimes in the energy denominators of NLO coefficients. For $\omega \sim \omega_Y$, the TPA spectrum $\mathrm{Im}\chi^{(3)}(-\omega, \omega, -\omega, \omega)$ reduces to a Lorentzian:

$$I(\omega) \propto \frac{|M(Y)|^2}{[E(Y) - 2\hbar\omega]^2 + \Gamma^2(Y)} , \qquad (18)$$

where $M(Y)$ is the transition moment (1). We expect $\Gamma(2\,^1A_g)$ to be small when $|2\,^1A_g\rangle$ is below E_g and hence metastable. All states at or above E_g can decay by dipole processes and are assigned equal widths. Conformational or disorder contributions to Γ are taken to be the same for all states; they are expected to increase on going from crystal to film to solution.

The simulated TPA spectra in Fig. 8 are based on PPP chains with $\delta = 0.15$, $N = 6$, 8, and 10, $E_g = 2.1$ eV, $\Gamma(2\,^1A_g)/E_g = 5\%$, and all other $\Gamma/E_g = 15\%$. Even for such short segments, the internal standard provided by E_g leads to similar spectra and the dominance of $|n\,^1A_g\rangle$ is readily apparent. The peak height was taken to be the same for all three spectra.

The fit is to an optical-quality PDA-4BCMU film[53,4] whose one-photon spectrum starts at 2.1 eV and peaks at 2.3 eV, thereby suggesting ~5% disorder broadening. The observed TPA spectrum starts at ~1.9 eV and shows a broad order-of-magnitude increase up to 3.0 eV. As $\hbar\omega$ approaches E_g, the transition moment $M(Y)$ in (1) diverges and both one- and two-photon processes occur. The onset of one-photon absorption limits the TPA measurement to around 3 eV and increases the experimental uncertainty of the high-energy points in Fig. 8. The simulated spectra confirm the greater intensity of the $1.5E_g$ feature and the weak TPA below E_g. The 15% broadening of $|n\,^1A_g\rangle$ in the film is slightly less than the 20% broadening that was used[8] for the 3WM data in solution.

Lifetime contributions have a larger role in two-photon resonances in THG. Near a two-photon resonance at $\omega=\omega_Y$, $\chi^{(3)}(-3\omega,\omega,\omega,\omega)$ has the same form as (18), except for replacing $|M(Y)|^2$ by

$$C(Y)=\langle Y|\mu|\phi(-\omega_Y)\rangle[\langle Y|\mu|\phi(-3\omega_Y)\rangle$$
$$+\langle Y|\mu|\phi(\omega_Y)\rangle]\,.\qquad(19)$$

When $3\hbar\omega$ exceeds E_g, the sum over virtual states in (1) may also diverge and requires additional $\Gamma(m\,^1B_u)$. In a dense spectrum two- and three-photon resonances overlap. For the most important processes with fields along the chain, lifetimes are readily included directly by using, say, the first 10 states in the A_g and B_u manifolds, finding all their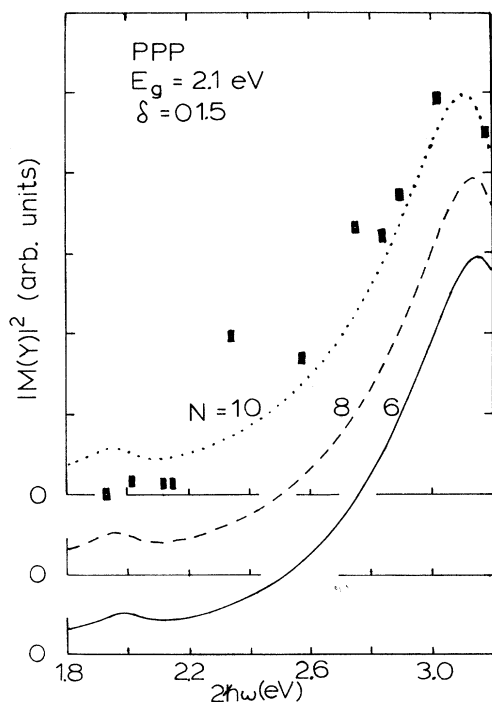 transition moments exactly, and summing over states explicitly. This procedure was used in Fig. 8. The same approach holds for $\chi^{(3)}(-2\omega,\omega,\omega,0)$ in EFISH and for $\chi^{(3)}(-\omega,\omega,0,0)$ in electroabsorption.

Sebastian and Weiser[9] pioneered the use of electroreflectance measurements on PDA crystals, primarily PTS and DCDH. A signal some 0.4 eV above E_g, or around $1.25E_g$, is assigned to one-photon transitions for electrons and holes at the band edge. The threshold for photoconduction[25] is in the same region, and the field dependence[54] of the poly[1,6-di(N-carbozolyl)-2,4-hexadiyne] (DCDH) sample was explicitly fit to a semiconductor model with free electrons and holes. Tokura et al.[10] assign A_g states at $1.24E_g$ based on electroreflectance studies at 77 K of PDA-TCDU crystals whose A and B forms have $E_g=2.292$ and 1.882 eV, respectively. As seen in Figs. 6 and 7, the TPA spectra of interacting π electrons primarily involve a few key even-parity states, rather than the full spectrum. The participation of band-edge states depends on their TPA cross sections and remains to be found.

B. σ-conjugated polysilanes

In contrast to the extensive work on σ-π separation in conjugated molecules,[30] σ-conjugated models for polysilanes[24] are still phenomenological and probably require more severe approximations. They nevertheless represent polymers with larger intrinsic alternation than possible in hydrocarbons and suggest a common model. The backbone of PS polymers[24] consists of $(Si)_n$ chains with $n>10^3$. Different $(RR'Si)_n$ polymers contain various alkyl and aryl substituents R. Two sp^3 hybrid orbitals per Si define the σ-conjugated backbone. We again have a half-filled band for $2N$ electrons in $2N$ orbitals for $N+1$ Si. The alternation is now intrinsic and distinguishes between intra- and interatomic transfer, with $t(1-\delta)$ for sp^3 orbitals of a Si atom and $t(1+\delta)$ for sp^3 orbitals forming a σ bond between adjacent Si. The on-site interaction $V(0)=9.04$ eV is based[55] on atomic data. Its somewhat smaller value, compared to C, reflects a larger orbital.

We have fit[47] E_g in a series of permethylsilanes to a PPP model with the same $t=-2.40$ eV used for polyenes and a larger alternation $\delta=\frac{1}{3}$. Now $|2\,^1A_g\rangle$ is above E_g in finite chains and remains 1.0 eV higher in the infinite polymer. These preliminary PPP parameters were chosen to interpret the observation of Thorne et al.[11] of a two-photon state 0.9 eV above E_g in poly(di-n-hexylsilane) (PDHS) in solution, in a film, and in a glass at low temperature. This strongly supports the sensitivity of $|2\,^1A_g\rangle$ to alternation in Fig. 7 and differs qualitatively from the single-particle result in Fig. 1.

The full TPA spectrum of PDHS films will be presented separately.[12] The $\delta=0.30$ spectrum in Fig. 7 is sufficient here. Larger alternation increases $E(2\,^1A_g)$ above $E_g=3.4$ eV in PDHS films. The $|2\,^1A_g\rangle$ band is at 4.15 eV at 300 K. There is another strong, broad TPA above 5 eV that we assign to the two-electron state.[12] The theoretical fit will reflect on $U=V(0)$, t, and δ for $(Si)_n$ chains. Tachibana et al.[13] report electroabsorption signals at 4.2 and 5.5 eV in PDHS at 77 K, with the

FIG. 8. TPA spectra, in units of $E_g=2.1$ eV, of PPP chains with $\delta=0.15$ and $N=6$, 8, and 10. The broadening in Eq. (18) is $\Gamma(2\,^1A_g)/E_g=5\%$ and $\Gamma/E_g=15\%$ for all other states. The TPA data for PDA-4BCMU films are from Ref. 53.

larger signal at 5.5 eV, that also support the present model. Both the TPA and the electroabsorption signal show temperature dependences that remain to be modeled. The important point is that even-parity states in such diverse systems may be modeled by the alternation dependence of PPP chains.

C. Polyenes and polyacetylene

There are several reasons for treating these important systems after presenting two-photon results for PDA's and for PS's. Recent work on polyene spectra[3] has focused on e-e correlations leading to $|2^1A_g\rangle$ below $|1^1B_u\rangle$. Exact solutions of PPP models account[19] for both the one- and two-photon gaps of gas-phase polyenes with $N=8$, 10, and 12. Such fits, to about 0.3 eV for excitations in the 3–5-eV range, are quite satisfactory for microscopic parameters based on other, smaller conjugated molecules. These parameters were used for all PPP calculations in Sec. II.

Recent solid-state work[22] on PA, on the other hand, has emphasized electron-phonon (e-p) coupling leading to self-localized states. The Su-Schrieffer-Heeger (SSH) model[56] retains noninteracting π electrons and treats E_g in PA as an adjustable parameter. Even so, the red edge of PA is sufficiently wide that the original gap of 1.4 eV has been taken as high as 1.8–1.9 eV in disorder[57] and instanton[58] models and as low as 1.1 eV in the three-dimensional structure.[59] Electroabsorption shows vibronic structure[60] and thus localized states in the red edges. The one-photon peak is at 1.9 and 2.1 eV in *trans*- and *cis*-PA, respectively.

These contrasting perspectives and associated arguments are beyond resolution without additional data, preferably on PA. The THG spectrum of Fann *et al.*[15] shows resonances around $E_g/3$ and $E_g/2$, with $E_g=1.8$ eV, and is consistent with the accumulation of both A_g and B_u states at E_g in Fig. 1. Single-particle theory accounts for the position[17] of the resonances, but differs by at least an order of magnitude for their relative intensities.

On the molecular side, fluorescence from polyenes in n-alkane matrices indicates[14] that $|2^1A_g\rangle$ remains below $|1^1B_u\rangle$; their separation in fact grows with increasing N, currently up to $N=16$, and $E(2^1A_g)$ extrapolates to $\sim E_g/2$ in PA, rather than to E_g according to single-particle analysis. The 2^1A_g feature in Fig. 6 shifts to lower energy with increasing N. To estimate the lowest TPA in PA, we extrapolate in Fig. 9 the ratio $E(2^1A_g)/E_g$ of the two- and one-photon excitations of PPP models with $\delta=0.07$. The corresponding experimental values are for 0-0 transitions in the gas phase[61] and in frozen-alkane solutions.[14] The principal difference is a red shift of ~ 0.4 eV for the more ionic $|1^1B_u\rangle$ state in solution. The experimental and theoretical $E(2^1A_g)/E_g$ in Fig. 9 extrapolates to 0.6–0.7, which is slightly higher than obtained from the ratio of the experimental extrapolations.[14]

Quite independently of the "correct" value of E_g in PA, we find $E(2^1A_g)\sim 0.65E_g$. Thus the two-photon resonance to $|2^1A_g\rangle$, whose amplitude $C(2^1A_g)$ is
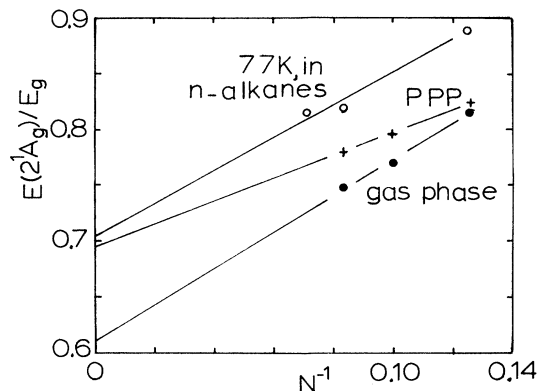

FIG. 9. Ratio $E(2^1A_g)/E_g$ of two- and one-photon gaps in PPP models of polyenes, with $\delta=0.07$. The gas-phase experimental values for $N=8$, 10, and 12 are from Ref. 61. The data in frozen-alkane solutions are from Ref. 14.

defined in (19), overlaps with the three-photon resonance at $E_g/3$. Very small lifetimes $\Gamma < 0.01$ eV are needed for all virtual states in order to resolve such closely spaced resonances. The observed width[15] of the $E_g/3$ feature is over 0.2 eV, more than enough to include $|2^1A_g\rangle$ and other A_g states close to the alternation gap.

In retrospect, the assignment of even-parity states simply from energy resonances, without regard to intensities, is extremely risky when the states are congested. The intense TPA in Fig. 6, for example, leads to a two-photon amplitude $C(n^1A_g)\sim 20C(2^1A_g)$. According to the sum rule (16), there is hardly any TPA intensity at higher energy, and there are no resonances[15] between 1.1 and 1.5 eV in the THG spectrum. The intensity information leads us to associate the 0.89-eV resonance with $|n^1A_g\rangle$, even though the even-parity states appear at E_g rather than $1.5E_g$ in isolated strands.

The Coulomb potential (11) of PPP models implies interactions between strands in PA microcrystals, at interchain contacts[62] of 3.9 Å. Even for nonoverlapping strands with $t_\perp=0$, we have π-electron dispersion (London) forces between neutral strands.[63] The exact PPP states of isolated polyenes serve as zeroth-order states. The shift of excitation energies due to charge fluctuations on adjacent strands corresponds to the gas-to-crystal shift in molecular exciton theory. We have carried out such a perturbation calculation[63] and find little or no shift for $E(2^1A_g)$, a red shift of ~ 0.3 eV for E_g, and a much larger red shift of ~ 1 eV for $|n^1A_g\rangle$. We suppose E_g to be ~ 2.0 eV, as found[14] for isolated strands in frozen alkane solutions, and $E(n^1A_g)=1.5E_g\sim 3$ eV for isolated strands. Interchain dispersion forces in PA then lead to similar energies around 1.8 eV for E_g and $E(n^1A_g)$. Although approximate, interchain dispersion rationalizes the THG spectrum within the PPP model used for polyenes, PDA's and PS's.

The similar ionicity and charge separation of $|G\rangle$ and $|2^1A_g\rangle$ in Tables II and III rationalize a negligible solid-state shift. The shift for the more ionic $|1^1B_u\rangle$ is comparable to the ~ 0.4-eV shift noted in Fig. 9 between the gas

phase and alkane solutions, but is due to π-electron dispersion rather than polarizability. The larger shift for $|n\,^1A_g\rangle$ is related to its greater charge separation in Table III. More precisely, $V(R)$ in (11) strongly couples the state $|Gn\,^1A_g\rangle$, in which one strand is excited, to the virtual state $|1\,^1B_u1\,^1B_u\rangle$, in which both are excited. Charge fluctuations of delocalized π electrons in adjacent conjugated strands thus shift the PPP excitations selectively and strongly stabilize the $|n\,^1A_g\rangle$.

The THG spectrum[15] of PA has also been discussed from other points of view. Wu and Kivelson[17] showed, using a field-theoretical approximation, that features at $E_g/3$ and $E_g/2$ occur naturally, although their relative intensities differ from experiment by at least an order of magnitude. Dixit, Guo, and Mazumdar[64] have recently argued, from exact transition moments of Hubbard and extended Hubbard models up to $N=8$, that the essential even-parity A_g state of the infinite chain is at E_g and is trapped between the first two B_u excitations for a wide variety of microscopic parameters like t, δ, U, or nearest-neighbor V. The contrast with our analysis is particularly striking at large δ and intermediate correlations, for instance in PS, where PPP models place both $|2\,^1A_g\rangle$ and $|n\,^1A_g\rangle$ well above E_g. Sinclair et al.[65] interpret THG in trans-PA in terms of quantum fluctuations[58] of the degenerate SSH ground state. The instanton model emphasizes differences between trans- and cis-PA. Wu and Sun[66] consider the effects of a random distribution of conjugation lengths. The relative roles of conjugation lengths, lattice fluctuations, e-e correlations, and interchain dispersion forces is not presently known. The well-separated strands and greater diversity of measurements in PDA's are advantageous for reconciling, at least qualitatively, molecular and polymeric data. PA is special, in our treatment, not because it is simple, but because it has important interchain interactions.

IV. DISCUSSION AND SUMMARY

Our initial survey of two-photon processes in conjugated polymers confirms the major predictions of PPP models. The contrast between the correlated TPA spectra in Figs. 6–8 and the single-particle spectrum in Fig. 1 deserves further discussion. The TPA transition moment $M(Y)$ in (1) diverges for $\hbar\omega_Y \geq E_g$, when the possibility of two-electron excitation across the gap is first realized for the single-particle states in Fig. 2. Additional two-photon absorptions are consequently expected in Fig. 1 at $2\hbar\omega/E_g \geq 2$. As noted in connection with PDA-4BCMU, however, this regime is precluded experimentally by overlapping one- and two-photon absorptions. There has been no reason to model TPA at such high energies.

The situation is completely different once e-e correlations are considered. The state derived from two-electron transfer across E_g may now occur below $2E_g$, in an experimentally accessible region. This is the only TPA in dimers and, as shown in (17), TPA in Hubbard dimers shifts to lower energy with increasing U in units of E_g. Intermediate e-e correlations in PPP chains shift the state derived from two-electron transfer to $\sim 1.5E_g$. Strong correlations $U \gg t$ shift it to $\sim E_g$ in Hubbard, PPP, or

other models whose ground state is purely covalent, with one electron per site.

The strong peaking of the one-photon spectrum is associated with delocalization in one-dimensional systems with small alternation. Dipole transition moments at E_g are precisely the ones contributing to $M(n\,^1A_g)$ in (1). The intensity and probable sharpness of the $|n\,^1A_g\rangle$ feature may therefore be understood in terms of the one-photon absorption. We have discussed additional phase arguments for the larger transition moment in Table III from $|1\,^1B_u\rangle$ to $|n\,^1A_g\rangle$ than to $|G\rangle$. The greater mean-square charge separation in $|n\,^1A_g\rangle$ provides a microscopic analysis directly for the correlated state. Such direct information is important in view of the qualitative nature of phase relations between a few configurations when many configurations are mixed.

A TPA below E_g in interacting models is clearly related to the vanishing alternation gap in regular Hubbard chains. The e-h symmetry of PPP chains leads to the same result and also holds for arbitrarily weak e-e interactions. For $\delta \sim 0$, the TPA intensity for $|2\,^1A_g\rangle$ and other states close to the alternation gap decrease with increasing correlations. The alternation gap may also exceed E_g, as shown in Fig. 7, for fixed e-e correlations. The larger δ and comparable correlations in polysilanes underscore this point.

The evolution of the single-particle spectrum in Fig. 1 with increasing e-e correlations may now be understood. For small δ, TPA appears below $E_g \sim 4t\delta$ at small U; the $U=2t$ spectrum in Fig. 5 indicates this red shift and the decreased intensity for the one-electron g-g and u-u processes in Fig. 2. Concomitantly, a strong new feature appears below $2E_g$ due to the red shift of the state derived from two-electron excitation. Both features shift to lower energy with increasing U/t and both lose intensity. TPA to spin waves at $\sim t^2/U$ becomes very weak for $U \gg t$ compared to TPA around $E_g = U$. Our results in the strong-coupling limit agree with those of Dixit, Guo, and Mazumdar.[64] The same general features occur for stronger correlations at larger δ. Although exciton formation leads to many possibilities at intermediate correlations, strong correlations eventually place $|2\,^1A_g\rangle$ below $|1\,^1B_u\rangle$.

We have merely alluded to vibronic (e-p) contributions. Side bands corresponding to C-C vibrations are typical of PDA spectra and provide rich structure in polyenes. The radiationless decay of excitons in PDA also points to e-p coupling. The primacy of e-p coupling in forming self-localized states[22] in conjugated polymers is the central theme of SSH theory, where e-e contributions are argued to be secondary. However, negative spin densities in PA, the different absorption of neutral and charged solitons, and other quantitative aspects require e-e contributions.

For two-photon spectra and other NLO processes e-e correlations are now central. These electronic responses are formally described by virtual rather than real states. Vibronic effects rather than real distortions are then important. Excited-state dynamics and decay will require e-p coupling. Just as in polyenes, the even-parity excited states of conjugated polymers are poorly represented in single-particle theory, even in the mean-field limit. In ad-

dition to the lowest A_g states at the alternation gap, the A_g states derived from two-electron excitation at E_g are now important and even dominant. Renormalization of microscopic parameters, so convenient for real excitations in SSH theory, cannot alter the single-particle spectrum in Fig. 1.

The NLO spectra of conjugated polymers, especially of PDA's, fully support the principal features of correlated models. We have so far retained PPP parameters for small molecules and have repeatedly exploited the internal standard provided by the one-photon gap E_g. More quantitative analysis of NLO spectra will undoubtedly require refined parameters, explicit treatment of e-p coupling, and specific modeling of the polymer and its side groups. Interchain charge fluctuations are particularly important in PA. Such studies are natural and challenging extensions to the two-photon spectra presented here for interacting π electrons in conjugated polymers.

ACKNOWLEDGMENTS

APPENDIX

We present here some Hückel results for neutral alternant hydrocarbons. The results are a consequence of topology and of a single-particle description, and do not depend on the particular choice of spin-independent potential. As such, they will hold also for Hartree-Fock (HF) and other single-particle solutions of Hubbard or PPP models for arbitrary size and alternation.

To provide a connection between site and orbital representations, we expand the site operators in the MO basis,

$$a_{p\sigma}^{\dagger} = \sum_{r} c_{pr} a_{r\sigma}^{\dagger} , \qquad (A1)$$

where c_{pr} is the (real) coefficient of site p in the rth MO. For the ground state, $|G_0\rangle$, where it is evident that C^+, C^-, $C\alpha$, and $C\beta$ sites are equally likely, the ionicity and charge-charge correlations on either sublattice take an especially simple form

$$\langle G_0 | q_j^2 | G_0 \rangle = \tfrac{1}{2} , \qquad (A2a)$$

$$\sum_{J} \langle G_0 | q_j q_{j+2n-1} | G_0 \rangle = -\tfrac{1}{2} , \qquad (A2b)$$

$$\langle G_0 | q_j q_{j+2n} | G_0 \rangle = 0 \quad (n \neq 0) . \qquad (A2c)$$

The neutrality condition $\sum_j q_j = 0$ is preserved. The presence of e-e interactions changes the ionicity (A2a) quantitatively as shown in Table II and discussed in Sec. II B.

We extend these results to excited states, and particularly to the states in Fig. 3. The ionicity of the determinants $|G_0\rangle$ and $|n\,^1A_0\rangle$ reduce to a sum over MO coefficients. The highest occupied and lowest unoccupied MO's obey the alternancy relations (6), and by use of (A1) we find, for all p,

$$\langle G_0 | q_p^2 | G_0 \rangle = \langle n\,^1A_0 | q_p^2 | n\,^1A_0 \rangle$$
$$= 2 \sum_{r,t} c_{pr}^2 c_{pt}^2 = \tfrac{1}{2} , \qquad (A3)$$

where the sums are over occupied MO's with spin α and β. The general result holds for single determinants and is readily evaluated for half-filled bands. Linear combinations show a strong dependence on the relative phases. For example, from (8) and (A1) we find

$$\langle 1\,^1B_0 | q_p^2 | 1\,^1B_0 \rangle = \tfrac{1}{2} + 2c_{p1}^4 , \qquad (A4)$$

while the triplet combination has instead a negative deviation from $\tfrac{1}{2}$. This is nothing more than the cell-model generalization of the $1s2s$ state of He, showing the closer approach of electrons in singlets, even for independent particles. $|2\,^1A_0\rangle$ is a linear combination of four determinants, two in phase and two out of phase, but now the cross terms cancel and the ionicity is again equal to $\tfrac{1}{2}$.

The one-electron transition moments to $|1\,^1B_0\rangle$ also reduce to sums over MO coefficients,

$$\langle G_0 | \mu | 1\,^1B_0 \rangle = \langle n\,^1A_0 | \mu | 1\,^1B_0 \rangle$$
$$= 2 \sum_{p} (-1)^p p c_{p1}^2 , \qquad (A5a)$$

$$\langle 2\,^1A_0 | \mu | 1\,^1B_0 \rangle = 2 \sum_{p} p c_{p1} c_{p2} , \qquad (A5b)$$

by making explicit use of alternancy symmetry. The result (A5a) reflects the fact that $|n\,^1A_0\rangle$ and $|G_0\rangle$ differ from $|1\,^1B_0\rangle$ by the same single e-h pair; $|2\,^1A_0\rangle$ also differs from $|1\,^1B_0\rangle$ by one e-h pair, and its transition moment to $|1\,^1B_0\rangle$ is comparable to that of $|G_0\rangle$ and $|n\,^1A_0\rangle$.

The variation of TPA matrix elements discussed in Sec. II D was related to the phases of single-particle states. We emphasized that $|2\,^1A_0\rangle$ and $|n\,^1A_0\rangle$ occurred with opposite phases in the states under consideration, and as shown in Table I. To demonstrate the importance of this, consider the following $\pm$ linear combinations:

$$|\pm\rangle = (|2\,^1A_0\rangle \pm |n\,^1A_0\rangle)/\sqrt{2} . \qquad (A6)$$

For small δ in short chains ($N < 12$), we have $n = 3$ and can see at once that

$$\langle \pm | q_p^2 | \pm \rangle = \tfrac{1}{2} \pm 4(-1)^p c_{p1}^3 c_{p2} \qquad (A7)$$

since both $|2\,^1A_0\rangle$ and $|n\,^1A_0\rangle$ have $Q = \tfrac{1}{2}$. The same analysis applies to $W(\pm)$ in (15), the value of which again hinges upon the relative sign of the cross terms. One combination enhances (reduces) correlations $\langle \pm | q_i q_{i+j} | \pm \rangle$ between nearby sites ($j < N/2$) and reduces (enhances) correlations between distant sites ($j > N/2$). Likewise, the transition moment to $|1\,^1B_0\rangle$ depends critically upon the phase of the linear combination, as can be seen below

$$\langle 1\,^1B_0 | \mu | \pm \rangle \propto \langle 1\,^1B_0 | \mu | 2\,^1A_0 \rangle \pm \langle 1\,^1B_0 | \mu | n\,^1A_0 \rangle . \qquad (A8)$$

Thus, from Table I and the phases in (A6), we see that reduced ionicity, charge separation, and transition moments go together in $|2\,^1A_g\rangle$, while the opposite is true for $|n\,^1A_g\rangle$.

[1] *Handbook of Conducting Polymers,* edited by T. A. Skotheim (Dekker, New York, 1986), Vols. 1 and 2; *Nonlinear Optical and Electroactive Polymers* edited by P. N Prasad and D. R. Ulrich (Plenum, New York, 1988).

[2] *Nonlinear Optical Properties of Organic Molecules and Crystals,* edited by D. S. Chemla and J. Zyss (Academic, New York, 1987), Vols. 1 and 2; these two volumes provide a comprehensive introduction to NLO in organics.

[3] B. S. Hudson, B. E. Kohler, and K. Schulten, in *Excited States,* edited by E. Lim (Academic, New York, 1982), Vol. 6, p. 1, and references cited therein.

[4] P. D. Townsend, W.-S. Fann, S. Etemad, G. L. Baker, J. Jackel, P. M. C. McWilliams, and Z. G. Soos (unpublished).

[5] B. E. Kohler and D. E. Schilke, J. Chem. Phys. **86**, 5214 (1987).

[6] G. L. Baker, S. Etemad, and F. Kajzar, SPIE Proc. **824**, 102 (1987).

[7] P. A. Chollet, F. Kajzar, and J. Messier, Synth. Met. **18**, 459 (1987); in *Nonlinear Optical and Electroactive Polymers* (Ref. 1), p. 121.

[8] R. R. Chance, M. L. Shand, C. Hogg, and R. Silbey, Phys. Rev. B **22**, 3540 (1980).

[9] L. Sebastian and G. Weiser, Chem. Phys. **62**, 447 (1981).

[10] Y. Tokura, Y. Oowaki, T. Koda, and R. H. Baughman, Chem. Phys. **88**, 437 (1984).

[11] J. R. G. Thorne, Y. Ohsako, R. M. Hochstrasser, and J. M. Zeigler, Chem. Phys. Lett. **162**, 455 (1989).

[12] Z. G. Soos and R. G. Kepler, Phys. Rev. B (to be published); K. G. Kepler and Z. G. Soos, Phys. Rev. B (to be published).

[13] H. Tachibana, Y. Kawabata, S. Koshihara, and Y. Tokura, Solid State Commun. **75**, 5 (1990).

[14] B. E. Kohler, C. Spangler, and C. Westerfield, J. Chem. Phys. **89**, 5422 (1988).

[15] W.-S. Fann, S. Benson, J. M. J. Madey, S. Etemad, G. L. Baker, and F. Kajzar, Phys. Rev. Lett. **62**, 1492 (1989).

[16] G. P. Agrawal, C. Cojan, and C. Flytzanis, Phys. Rev. B **17**, 776 (1978).

[17] W. Wu and S. Kivelson, Synth. Met. **28**, D575 (1989); W. Wu, Phys. Rev. Lett. **61**, 1119 (1988).

[18] Z. G. Soos, P. C. M. McWilliams, and G. W. Hayden, Chem. Phys. Lett. **171**, 14 (1990).

[19] Z. G. Soos and G. W. Hayden, in *Electroresponsive Molecular and Polymeric Systems,* edited by T. Skotheim (Dekker, New York, 1988), p. 197.

[20] J. R. Heflin, K. Y. Wong, O. Zamani-Khamiri, and A. F. Garito, Phys. Rev. B **38**, 1573 (1988).

[21] Z. G. Soos and S. Ramasesha, J. Chem. Phys. **90**, 1067 (1989); S. Ramasesha and Z. G. Soos, Chem. Phys. Lett. **153**, 171 (1988).

[22] A. J. Heeger, S. Kivelson, J. R. Schrieffer, and W. P. Su, Rev. Mod. Phys. **60**, 781 (1988).

[23] *Polydiacetylenes,* Vol. 102 of *NATO Advanced Study Institute Series E,* edited by D. Bloor and R. Chance (Martinus Najhoff, the Netherlands, 1985); *Crystallographically Ordered Polymers, ACS Symposium Series 337,* edited by D. J. Sandman (American Chemical Society, Washington, D.C., 1987).

[24] K. S. Schweizer, L. A. Harrah, and J. M. Zeigler, in *Proceedings of the International Workshop on Silicon-Based Polymer Science,* edited by J. M. Ziegler and G. Fearon (American Chemical Society, Washington, D.C., 1990), and references cited therein; J. Michl, J. W. Downing, T. Karatsu, K. A. Klingensmith, G. M. Wallraff, and R. D. Miller, in *Inorganic and Organometallic Polymers, ACS Symposium Series 360,* edited by M. Zeldin, K. J. Wynne, and H. R. Allcock (American Chemical Society, Washington, D.C., 1988), p. 61.

[25] K. Lochner, B. Reimer, and H. Bassler, Phys. Status Solidi **766**, 533 (1976); R. R. Chance and R. H. Baughman, J. Chem. Phys. **64**, 3889 (1976).

[26] R. G. Kepler, J. M. Zeigler, L. A. Harrah, and S. R. Kurtz, Phys. Rev. B **35**, 2818 (1987).

[27] D. C. Hanna, M. A. Yuratich, and D. Cotter, *Nonlinear Optics of Free Atoms and Molecules* (Springer, Berlin, 1979).

[28] Y. R. Shen, *The Principles of Nonlinear Optics* (Wiley, New York, 1984).

[29] P. W. Langhoff, S. T. Epstein, and M. Karplus, Rev. Mod. Phys. **44**, 602 (1972).

[30] L. Salem, *The Molecular Orbital Theory of Conjugated Systems* (Benjamin, New York, 1966); a thorough and accessible discussion of work up to 1965.

[31] A. D. McLachlan, Mol. Phys. **2**, 276 (1959); S. R. Bondeson and Z. G. Soos, Chem. Phys. **44**, 403 (1979); O. J. Heilmann and E. H. Lieb, Trans. N.Y. Acad. Sci. Ser. II **33**, 116 (1971).

[32] J. Hubbard, Proc. R. Soc. London Ser. A **276**, 238 (1963); **277**, 237 (1964); **281**, 401 (1964).

[33] R. Pariser and R. G. Parr, J. Chem. Phys. **21**, 767 (1953); J. A. Pople, Trans. Faraday Soc. **42**, 1375 (1953); see also *The Molecular Orbital Theory of Conjugated Systems* (Ref. 30).

[34] K. Ohno, Theor. Chim. Acta **2**, 219 (1964).

[35] A. Painelli and A. Girlando, Synth. Met. **27**, A15 (1988); D. K. Campbell, J. Tinka Gamel, and E. Y. Loh, Jr., *ibid.* **27**, A9 (1988); Phys. Rev. B **38**, 12043 (1988); S. Kivelson, W. P. Su, J. R. Schrieffer, and A. J. Heeger, Phys. Rev. Lett. **58**, 1899 (1987); D. Baeriswyl, P. Horsch, and K. Maki *ibid.* **60**, 70 (1988).

[36] Z. G. Soos and S. Ramasesha, in *Valence Bond Theory and Chemical Structure,* edited by D. J. Klein and N. Trinajstic (Elsevier, Amsterdam, 1990), p. 81, and references cited therein.

[37] S. Mazumdar and Z. G. Soos, Synth. Met. **1**, 77 (1979).

[38] G. Rumer, Göttingen Nachrich. Tech. **1932**, 377.

[39] Z. G. Soos, S. Kuwajima, and J. E. Mihalick, Phys. Rev. B **32**, 3124 (1985); K. Chang, I. Affleck, G. W. Hayden, and Z. G. Soos, J. Phys. Condens. Matter **1**, 153 (1989).

[40] S. Ramasesha and Z. G. Soos, J. Chem. Phys. **80**, 3278 (1984).

[41] A. A. Ovchinnikov, Zh. Eskp. Teor. Fiz. **57**, 2137 (1970) [Sov. Phys. JETP **30**, 1160 (1970)].

[42] M. Takahashi, Prog. Theor. Phys. **42**, 1098 (1969); **42**, 1619 (1970).

[43] E. H. Lieb and F. Y. Wu, Phys. Rev. Lett. **20**, 1445 (1968).

[44] J. C. Bonner and H. W. J. Blöte, Phys. Rev. B **25**, 6959 (1982), and references cited therein.

[45] Z. G. Soos and S. R. Bondeson, in *Extended Linear Chain Compounds,* edited by J. S. Miller (Plenum, New York, 1983), Vol. 3, p. 193.

[46] G. W. Hayden and E. J. Mele, Phys. Rev. B **34**, 5484 (1986); D. Baeriswyl and K. Maki *ibid.* **31**, 6633 (1985); J. E. Hirsch and M. Grabowski, Phys. Rev. Lett. **52**, 1713 (1984); S. Mazumdar and S. N. Dixit, Synth. Met. **28**, D463 (1989).

[47] Z. G. Soos and G. W. Hayden, Chem. Phys. **143**, 199 (1990).

[48] V. Enkelmann, in *Polydiacetylenes, Advances in Polymer Science,* edited by H. J. Cantow (Springer-Verlag, Berlin, 1984), Vol. 63, p. 137.

[49] M. J. Nowak, G. J. Blanchard, G. L. Baker, S. Etemad, and Z. G. Soos, Phys. Rev. B **41**, 7939 (1990).

[50] G. M. Carter, J. V. Hryniewicz, M. K. Thakur, Y. J. Chen, and S. E. Meyler, Appl. Phys. Lett. **49**, 998 (1986); B. I. Greene, J. Orenstein, R. R. Millard, and L. R. Williams, Phys. Rev. Lett. **58**, 2750 (1987).

[51] L. Sebastian and G. Weiser, Chem. Phys. Lett. **64**, 396 (1979).

[52]M. Lequime and J. Hermann, Chem. Phys. **26**, 431 (1977); B. Reimer and H. Bassler, Chem. Phys. Lett. **55**, 315 (1978).

[53]W.-S. Fann, Ph.D. thesis, Stanford University, 1990.

[54]L. Sebastian and G. Weiser, Phys. Rev. Lett. **46**, 1156 (1981).

[55]A. Herman, Chem. Phys. **122**, 53 (1988).

[56]W. P. Su, J. R. Schrieffer, and A. J. Heeger, Phys. Rev. Lett. **44**, 1698 (1979); Phys. Rev. B **22**, 2099 (1980); **28**, 1138(E) (1983).

[57]S. Etemad, G. L. Baker, C. B. Roxlo, B. R. Weinberger, and J. Orenstein, Mol. Cryst. Liq. Cryst. **117**, 275 (1985).

[58]J. Yu, H. Matsuoka, and W. P. Su, Phys. Rev. B **37**, 10 367 (1988).

[59]P. Vogl, D. K. Campbell, and O. F. Sankey, Synth. Met. **28**, D513 (1989).

[60]S. D. Phillips, R. Worland, G. Yu, T. Hagler, R. Freedman, Y. Cao, V. Yoon, J. Chiang, W. C. Walker, and A. J. Heeger, Phys. Rev. B **40**, 9751 (1989).

[61]K. L. D'Amico, C. Manos, and R. L. Christensen, J. Am. Chem. Soc. **102**, 1777 (1980).

[62]H. Kahlert, O. Leitner, and G. Leising, Synth. Met. **17**, 467 (1987).

[63]Z. G. Soos, G. W. Hayden, P. C. M. McWilliams, and S. Etemad, J. Chem. Phys. **93**, 7439 (1990).

[64]S. N. Dixit, D. Guo, and S. Mazumdar, Phys. Rev. B **43**, 6781 (1991).

[65]M. Sinclair, D. Moses, D. McBranch, A. J. Heeger, J. Yu, and W. P. Su, Synth. Met. **28**, D655 (1989).

[66]C.-q. Wu and X. Sun, Phys. Rev. B **42**, 9736 (1990).